



# CHORUS

This is the accepted manuscript made available via CHORUS. The article has been published as:

## Controlled growth of Gd-Pt surface alloys on Pt(111)

Marta Przychodnia, Michał Hermanowicz, Emil Sierda, Micha Elsebach, Tomasz Grzela,  
Roland Wiesendanger, and Maciej Bazarzik

Phys. Rev. B **105**, 035416 — Published 13 January 2022

DOI: [10.1103/PhysRevB.105.035416](https://doi.org/10.1103/PhysRevB.105.035416)

# Controlled growth of Gd-Pt surface alloys on Pt(111)

Marta Przychodnia,<sup>1,2,\*</sup> Michał Hermanowicz,<sup>1,3</sup> Emil Sierda,<sup>2</sup> Michał Elsebach,<sup>2</sup> Tomasz Grzela,<sup>1</sup> Roland Wiesendanger,<sup>2</sup> and Maciej Bazarnik<sup>1,2,†</sup>

<sup>1</sup>*Institute of Physics, Poznan University of Technology, Piotrowo 3, 60-965 Poznan, Poland.*

<sup>2</sup>*Department of Physics, University of Hamburg, Jungiusstrasse 11, D-20355 Hamburg, Germany.*

<sup>3</sup>*Interdisciplinary Centre for Mathematical and Computational Modelling, University of Warsaw, Tyńiecka 15/17, 02-630 Warsaw, Poland.*

(Dated: December 22, 2021)

In this paper we are reporting on the structural and electronic properties of Gd-Pt surface alloys grown on a Pt(111) substrate. Using scanning tunneling microscopy and spectroscopy combined with density functional theory calculations, we are exploring differences between three different surface alloys, identified as single-layer GdPt<sub>2</sub>, single-layer GdPt<sub>5</sub>, and double-layer GdPt<sub>5</sub>. We show that an appropriate choice of substrate temperature as well as surface coverage with Gd atoms allows for selective growth of all observed surface structures.

## I. INTRODUCTION

Rare earth metals (REMs) have been the subject of great interest mainly because of their peculiar magnetic properties. The magnetism originates from strongly localized  $4f$  electrons shielded by  $5d$  and  $6s$  valence electrons. These conduction electrons couple chemically inert  $4f$  electrons *via* an indirect Ruderman-Kittel-Kasuya-Yosida (RKKY) exchange interaction. Bulk alloys of REMs with transition metals and noble metals, were investigated for many years in terms of their structural [1, 2], chemical [1], electronic [3–5] and magnetic [1, 4–7] properties. Gd-based alloys, in particular, are treated as model systems because of their large magnetic moments resulting from the half-filled  $4f$  shells [8, 9]. The observed increase of the Curie temperature ( $T_C$ ) in Gd thin films [10–12] and the dependence of the  $5d$  band structure on the film thickness [13] resulted in increasing interest in investigations of on-surface structures [14, 15], thin films [9, 16–23], and surface compounds [24–27] of REMs. Recent reports on surface alloys of REMs e.g. (Gd, Ce) with noble metals (Au, Ag, Pt) established them as a new class of stable and ordered 2D magnets [26–29]. They exhibit a characteristic moiré pattern that results from a mismatch between substrate lattice and surface alloy overlayers. Surface alloys of REMs with Au or Ag form a REM-Au<sub>2</sub> and REM-Ag<sub>2</sub> monolayer on top of the noble metals (111) substrates upon saturation [27, 28, 30, 31]. These structures were already investigated as templates for the growth of magnetic Co-nanodot arrays [28, 30, 32–35] and organic polymers [36, 37]. In contrast, REM-Pt alloys exhibit a more complicated structure of alternating kagomé lattices of Pt atoms and hexagonal REM-Pt<sub>2</sub> layers [25, 38, 39]. Depending on the surface termination, clearly distinguishable structural, chemical, and magnetic properties are obtained. Alloy structures terminated with a kagomé Pt

overlayer are less reactive than these terminated with a REM-Pt alloy layer [40]. So far, there are only a few reports on alloying Pt with REMs investigating mainly the weakening of the O–H binding on the surface of these alloys compared to pure Pt for development of catalysts with enhanced activity of oxygen-reduction reaction and long-term stability in proton exchange membrane fuel cells [41–43].

In this paper, we report on the controlled growth as well as structural and electronic properties of Gd-Pt surface alloys on Pt(111) investigated using scanning tunneling microscopy (STM) and spectroscopy (STS) techniques supplemented by density functional theory (DFT) calculations. STM imaging with atomic resolution allows for an unambiguous determination of the terminating layer. We study the growth mode in dependence of substrate temperature during the reactive growth as well as surface coverage with Gd atoms from sub-monolayer to two monolayers. Our analysis reveals three distinct alloy structures, corresponding to different numbers of alternating hexagonal GdPt<sub>2</sub> and kagomé Pt layers.

## II. EXPERIMENTAL METHODS

The STM and STS experiments were performed in a multi-chamber ultra-high vacuum system with a base pressure of  $5.0 \times 10^{-11}$  mbar equipped with a home-built variable-temperature STM (VT STM) [44]. The Pt(111) single-crystal substrate with a purity of 99.999%, was supplied by MaTecK, GmbH, Germany. It was cleaned by cycles of Ar-ion bombardment, heating in an oxygen atmosphere ( $p_{O_2} = 5.0 \times 10^{-8}$  mbar), and flashing up to 1300 K. Before Gd deposition, the Pt(111) substrate was characterized using STM imaging, STS, Auger electron spectroscopy, and low-energy electron diffraction techniques to verify the surface cleanliness. Gd was evaporated from a tungsten crucible, using an e-beam evaporator, onto the substrate held at temperatures ranging from room temperature (RT) to 926 K. The samples used to analyze the temperature dependence of the area oc-

\* marta.przychodnia@put.poznan.pl

† maciej.bazarnik@put.poznan.pl

cupied by the different alloys were prepared by reactive growth at a substrate temperature of 865 K and subsequent post-annealing for 15 minutes at higher temperatures of up to 926 K. During the deposition processes, the background pressure did not exceed  $1.0 \times 10^{-10}$  mbar. To preserve the same level of Gd diffusion into the bulk for coverage-dependence analysis, we increased only the deposition rate, while the deposition time was kept constant. For STM data analysis, we assigned the coverage ( $\theta$ ) of one monolayer ML to the amount of deposited Gd necessary to cover the sample surface completely with a GdPt<sub>5</sub> alloy yielding 3.75 Gd atoms per nm<sup>2</sup>. After the deposition, the samples were kept at the deposition temperature for 15 minutes. To ensure reproducible deposition conditions, we controlled the substrate temperature in two different ways: by calibration of the heating stage based on a thermocouple readout, and by an externally mounted pyrometer focused on the sample. Afterward, the samples were transferred *in vacuo* into the STM and cooled to the measurement temperature of 30 K. Electrochemically etched tungsten tips cleaned by standard *in situ* procedures were used for the STM studies. All topographic data were obtained in constant-current mode and processed using Gwyddion software [45]. Tunneling spectra were recorded in constant-height mode after tip stabilization at given parameters, i.e. bias ( $U$ ) and tunneling current ( $I$ ). The differential tunneling conductance ( $dI/dU$ ) was measured *via* lock-in technique by applying modulation voltage to the sample bias voltage with a peak-to-peak value  $U_{p_k-p_k} = 50$  mV and a frequency  $\nu = 6.8$  kHz. For each analyzed alloy, the presented spectroscopy data results from averaging 40 curves measured with certain tip positions within the moiré pattern to improve the signal-to-noise ratio [46]. The normalization of the measured  $dI/dU$  signal over  $I/U$  allows us to compare directly with the local density of states (DOS) of the calculated electronic structure [47, 48]. At the measurement temperature of 30 K, we do not observe any features around Fermi energy in the raw  $dI/dU$  data. At the same time, the above mentioned normalization procedure leads to artifacts around zero bias, therefore, the region from -0.01 V to 0.01 V in the presented spectroscopy data has been omitted. For the DFT calculations we used a single surface unit cell of an alloy on top of 25 MLs of Pt (see Fig. 2). We choose the thickness of the slab following Wiebe *et al.* [49] to accurately model the Pt(111) surface. Geometry optimization was performed within the local density approximation (LDA) using the Broyden-Fletcher-Goldfarb-Shanno (BFGS) method as implemented in the Quantum Espresso code [50, 51]. For the calculation of single-layer GdPt<sub>2</sub> (1L GdPt<sub>2</sub>) and single-layer GdPt<sub>5</sub> (1L GdPt<sub>5</sub>), three surface MLs were allowed to relax during the calculations. In case of double-layer GdPt<sub>5</sub> (2L GdPt<sub>5</sub>), five MLs were allowed to relax. The spin-polarized partial density of states (PDOS) has been calculated within the Perdew-Burke-Ernzerhof generalized gradient approximation (PBE-GGA) for the exchange-correlation func-

tional as implemented in the Siesta software package [52–54]. All the Siesta calculations have been performed using a double-zeta basis set with polarization orbitals and with the surface Brillouin zone sampled at a  $16 \times 16 \times 1$  Monkhorst-Pack k-points grid (a finer grid of  $36 \times 36 \times 1$  k-points has been used for PDOS). The presented PDOS graphs show separately the  $s$ ,  $p$  and  $d$  states of Pt and Gd and, in the latter case, also the  $f$  states. Data are summed over all atoms residing in the terminating layer and, in case of GdPt<sub>5</sub>, in the first Gd layer. Magnetic moments were calculated using the Mulliken charge analysis.

### III. RESULTS AND DISCUSSION

Deposition of Gd onto a clean Pt(111) substrate at RT does not lead to ordered structures, similarly to prior observations for the Ce-Pt system [38, 55]. Under these conditions, Gd forms irregular and randomly distributed clusters and islands with 150-230 pm apparent height. Below alloy-formation temperature, Gd and Pt atoms intermix and form irregularly shaped islands, when reactive growth is involved. Ordered structure formation, regardless of Gd coverage and annealing time, starts above 750 K. This minimum substrate temperature is consistent with earlier observations by Ulrikkeholm *et al.* [56] on alloy formation of a 2 nm thick Gd overlayer deposited onto Pt(111) substrate, for which temperatures in the range between 723 K and 773 K were needed.

The STM images presented in Fig. 1 show three different ordered structures. Depending on the sample preparation parameters, the fraction of surface coverage for each of these structures can be controlled. Based on their structural properties as well as correlation between the growth parameters and the fraction of surface occupied by each of the structures, we identified them as single-layer GdPt<sub>2</sub>, single-layer GdPt<sub>5</sub>, and double-layer GdPt<sub>5</sub>. Below we present analysis of the structural and electronic properties of each of these alloys confirming our assignment.

Models of all three alloys are presented in Fig. 1 (a). The distances between individual layers are exaggerated to show the termination layer of each alloy more clearly. 1L GdPt<sub>2</sub> is terminated with a REM-Pt layer similar to GdAu<sub>2</sub> or GdAg<sub>2</sub> [26, 27]. Both single- and double-layer GdPt<sub>5</sub> are terminated by a Pt kagomé lattice with the REM-Pt layer being submerged. Note that below the bottom GdPt<sub>2</sub> layer we expect to have a pure Pt(111) substrate. The DFT calculations indicate that the Pt(111) substrate layer is energetically favorable by 1.27 eV over a Pt(111) layer plus kagomé interlayer.

In our experiments, each alloy shows long-range and short-range order. There are many defects in the long-range structure of 1L GdPt<sub>2</sub> and undisturbed moiré areas are not bigger than several tens of nm<sup>2</sup>, which influences the exact determination of the unit cell. However, an approximate moiré unit cell as marked in Fig.

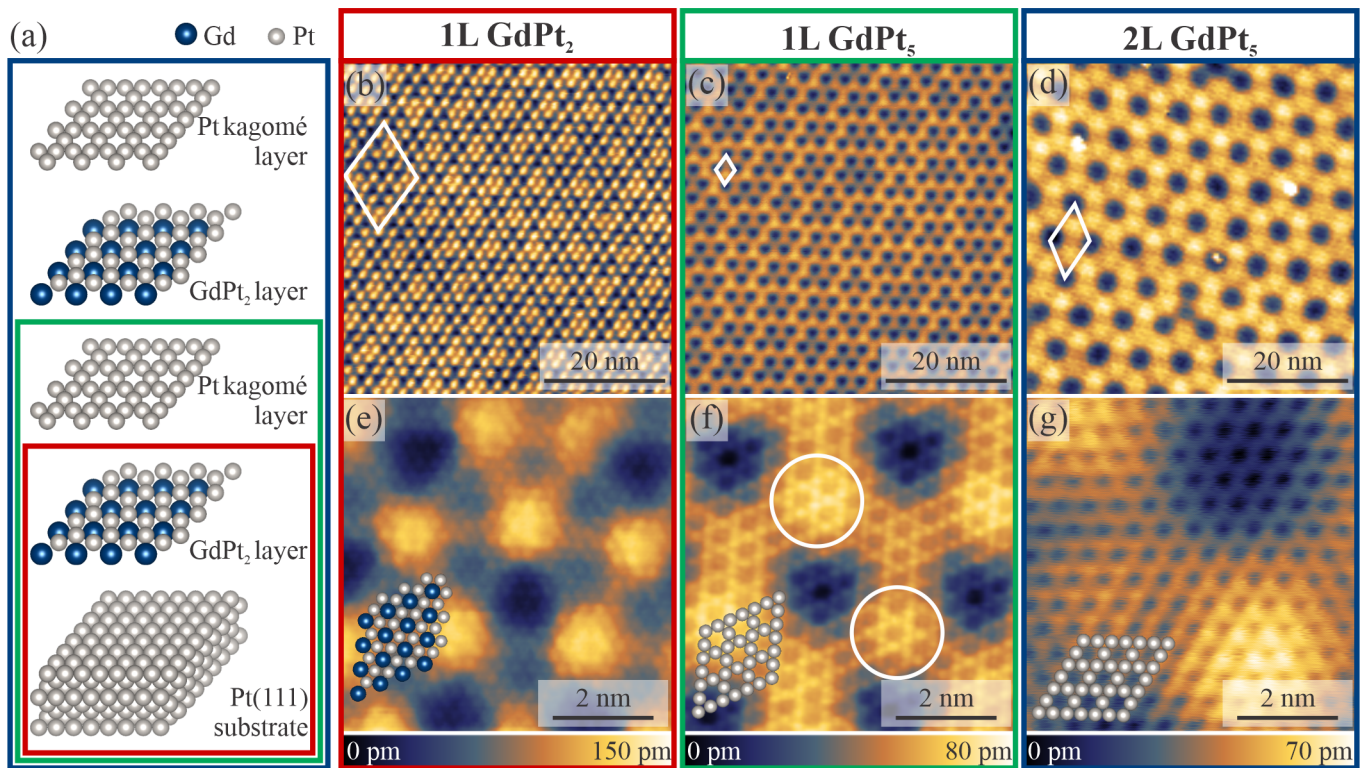


FIG. 1. Gd-Pt surface alloy structures. (a) Model with the individual layers separated for clarity. Color boxes relate the atomic structure of the surface alloys with their corresponding STM images. (b), (c), and (d) are large-scale STM topography images of 1L GdPt<sub>2</sub>, 1L GdPt<sub>5</sub>, and 2L GdPt<sub>5</sub> respectively. The apparent moiré lattice unit cells are marked on each image. The panels (e), (f), and (g) show zoomed in images of each surface alloy with atomic resolution of the termination layer. 1L GdPt<sub>2</sub> (e) has a hexagonal atomic lattice, while 1L GdPt<sub>5</sub> (f) and 2L GdPt<sub>5</sub> (g) exhibit a kagomé atomic lattice. Tunneling parameters: (b)  $I = 1$  nA,  $U = 0.5$  V; (c)  $I = 1$  nA,  $U = 0.5$  V; (d)  $I = 100$  pA,  $U = 1.5$  V; (e)  $I = 50$  nA,  $U = -1$  mV; (f)  $I = 100$  nA,  $U = -1$  mV; (g)  $I = 100$  pA,  $U = 35$  mV.

1 (b) has a periodicity  $d_{\text{moiré-1LGdPt}_2} = (14.7 \pm 0.1)$  nm. The number of defects points to considerable stress in this alloy. In atomically resolved STM images (see Fig. 1 (e)), a hexagonal lattice with interatomic distances  $d_{\text{NND-1LGdPt}_2} = (320 \pm 8)$  pm is visible, corresponding to the nearest neighbor distance (NND) in 1L GdPt<sub>2</sub>. The Gd-Gd distance equals to  $d_{1\text{LGdPt}_2} = (555 \pm 14)$  pm. The corresponding lattice constant of the GdPt<sub>2</sub> layer in bulk GdPt<sub>5</sub> is 529 pm [42]. In the case of few nanometer thick alloy layers, this value increases to 533 pm [56]. Therefore, the thinner the film is, the larger is the lattice constant, which is consistent with our experimental results. This accounts for the stress in the alloy and the formation of many dislocation lines and other irregularities in the moiré pattern. We have observed that on samples, where all three alloy structures coexist, impurity adsorption is preferred on 1L GdPt<sub>2</sub> over 1L GdPt<sub>5</sub> or 2L GdPt<sub>5</sub>, suggesting a higher chemical reactivity of the uncovered GdPt<sub>2</sub> layer.

As the STM image in Fig. 1 (c) shows, the structure of 1L GdPt<sub>5</sub> is much more ordered compared to 1L GdPt<sub>2</sub>, with lower apparent corrugation and less visible line defects. The moiré size is much smaller with  $d_{\text{moiré-1LGdPt}_5} = (2.87 \pm 0.04)$  nm. However, on close

inspection, details differ between the distinct "on-top" sites, as marked in Fig. 1 (f), pointing to the incommensurate nature of the alloy and the underlying substrate lattice. This zoom-in image reveals a kagomé lattice with an atomic distance of  $d_{\text{NND-1LGdPt}_5} = (269 \pm 4)$  pm and a unit cell size of  $d_{1\text{LGdPt}_5} = (537 \pm 4)$  pm. This corresponds to the Pt kagomé termination layer as seen in the model (Fig. 1 (a)). The Gd atoms in the sublayer are positioned in the vacancies of the Pt kagomé lattice. The Pt NND is shorter than in Pt(111) which is in accordance with previous studies [42].

The third observed structure depicted in Fig. 1 (d) shows the highest degree of ordering with the lowest number of defects and a moiré unit cell with  $d_{\text{moiré-2LGdPt}_5} = (6.6 \pm 0.2)$  nm. The apparent corrugation of 2L GdPt<sub>5</sub> is very similar to that of 1L GdPt<sub>5</sub>. However, the atomic lattice relaxes yielding a unit cell size of  $d_{2\text{LGdPt}_5} = (544 \pm 2)$  pm (Fig. 1 (g)). The double-layer preserves the platinum termination with its kagomé lattice having an atomic distance of  $d_{\text{NND-2LGdPt}_5} = (272 \pm 2)$  pm. It is important to point out that the double-layer is sufficient to relax the structure and avoid the formation of dislocation lines. The coverage dependence study presented below allowed

for an unambiguous identification of 1L GdPt<sub>5</sub> and 2L GdPt<sub>5</sub>.

The 1L GdPt<sub>2</sub> is the most strained among all observed structures, with Gd pushed out of the plane of Pt atoms. Here, the unit cell is the largest and it becomes smaller when the formation of 1L GdPt<sub>5</sub> is completed with a Pt kagomé lattice layer above the Gd. The moiré pattern becomes more ordered when the second layer of GdPt<sub>5</sub> is formed, while the alloy unit cell observed in our experiments is still larger than the bulk value of 529 pm [42]. In our DFT calculations, the Gd atoms are pushed out of the GdPt<sub>2</sub> layer by the Pt atoms in the layer below (see the models in Fig. 2). This state is preserved in 1L GdPt<sub>5</sub> on top of Pt(111) as well as in 2L GdPt<sub>5</sub>.

To investigate the electronic properties of all three alloys, we turn to the combination of STS and DFT. We obtained spectra across the apparent moiré and averaged them to allow for a comparison with the DFT results. The variations within the moiré pattern are small and show slight differences in the intensity of observed STS peaks[46], but the main features remain. Figure 2 summarizes experimental STS data and calculated DOS of the terminating layer for all three alloys. In all three cases, the spectroscopic features are well-reproduced. However, their energy is underestimated by DFT. The unoccupied state of GdPt<sub>2</sub> and the occupied state of 1L and 2L GdPt<sub>5</sub> are closer to the Fermi energy than in the experiment.

Figure 3 summarizes the calculated PDOS for all three alloy structures. Comparison of the experimental data with DFT calculations confirms our interpretation of the structural composition of the observed surface alloys. For 1L GdPt<sub>2</sub>, the most pronounced experimental peak is located at 2.5 V originating from the exposed Gd. Since the 4*f* shell has a sharp drop off into the vacuum in the experiment, most likely we tunnel into a combination of 5*d* and 6*s* states. The other experimental peak at 1.42 V coincides with the second peak in the 5*d* band. However, it is unclear why the intensity of those two peaks is so different in the experimental STS data. Both, experimental data and the PDOS do not show sharp distinct features in the occupied states. Instead, they show a slow increase in intensity that can be attributed to a combination of Pt and Gd states. At the same time, for GdPt<sub>5</sub>, the intensity originating from Gd is suppressed with only small features visible in the unoccupied states that are also evident for 2L GdPt<sub>5</sub>. This can readily be explained as Gd is submerged below the Pt kagomé. Experimentally, the highest intensity for both 1L GdPt<sub>5</sub> and 2L GdPt<sub>5</sub> is observed in the occupied states around -3.1 V. In the calculated PDOS, the highest intensity in the Pt 5*d* band is shifted towards the Fermi level to -1.8 V. The dominance of the Pt features was expected due to the Pt termination layer. DFT shows considerable spin asymmetry of Gd atoms due to the interaction of the 5*d* shell with the 4*f* shell. Pt states close to the energy of the Gd 4*f* peak are also spin-polarized. The PDOS plots with a wider energy range are shown in Supplemental Material

TABLE I. Calculated magnetic moments. Layers in the first column are ordered analogously to layers in Fig. 1 (a).

| Layer                           | Atom | 1L GdPt <sub>2</sub> | 1L GdPt <sub>5</sub> | 2L GdPt <sub>5</sub> |
|---------------------------------|------|----------------------|----------------------|----------------------|
| Pt kagomé                       | Pt   | -                    | -                    | 0.01 $\mu_B$         |
| GdPt <sub>2</sub>               | Pt   | -                    | -                    | 0.09 $\mu_B$         |
|                                 | Gd   | -                    | -                    | 7.62 $\mu_B$         |
| Pt kagomé                       | Pt   | -                    | 0.10 $\mu_B$         | 0.10 $\mu_B$         |
| GdPt <sub>2</sub>               | Pt   | 0.03 $\mu_B$         | 0.12 $\mu_B$         | 0.06 $\mu_B$         |
|                                 | Gd   | 7.64 $\mu_B$         | 7.58 $\mu_B$         | 7.61 $\mu_B$         |
| substrate 1 <sup>st</sup> layer | Pt   | 0.10 $\mu_B$         | 0.09 $\mu_B$         | 0.06 $\mu_B$         |
| substrate 2 <sup>nd</sup> layer | Pt   | 0.05 $\mu_B$         | 0.02 $\mu_B$         | 0.02 $\mu_B$         |

[46].

The calculated magnetic moments of all three alloys are summarized in Table I. Strikingly, 1L GdPt<sub>2</sub> has very small induced magnetic moments of the Pt atoms in the Gd plane. In both GdPt<sub>5</sub> surface alloys, the magnetic moments of all Pt atoms around the Gd atoms are similar to 1L GdPt<sub>2</sub>, but the drop towards the bulk of the substrate is sharper. 2L GdPt<sub>5</sub> has a slightly lower magnetic moment per Pt atom compared to 1L GdPt<sub>5</sub>. In bulk, GdPt<sub>5</sub> is ferromagnetic [57], however, due to the thickness confinement and the stress in the atomic lattice the magnetic character of these alloys can be different. This yet remains to be experimentally addressed.

In the following, the control and selectivity of the growth process will be addressed. Analysis of a large variety of samples, obtained under variable preparation conditions, proves that the occurrence and the surface area covered by the three different surface alloys depend on two parameters, i.e. the surface coverage of Gd and the substrate temperature during the reactive growth process. In all cases, we investigate the samples globally obtaining data for different macroscopic positions of the STM probe for a total area of at least 1.5  $\mu\text{m}^2$ .

In the Gd coverage regime between 0.2 ML and 0.5 ML, we observe the coexistence of 1L GdPt<sub>2</sub>, 1L GdPt<sub>5</sub>, and disordered Gd-Pt clusters. For the lowest investigated Gd coverage (0.2 ML), we observe hampering of surface alloy growth when the substrate temperature exceeds 900 K. The intermixing process is enhanced, hence diffusion of Gd atoms into the bulk increases and Pt-overlayer formation occurs. In consequence, the on-surface Gd concentration is too low to form surface alloys, and we observe only Gd-Pt clusters and islands with unknown stoichiometry. When the Gd coverage is below 0.75 ML, we do not find any clear temperature dependence of the analyzed surface alloys in the range from 865 K to 926 K. Analysis of numerous STM images shows that the surface morphology strongly varies across the sample.

A detailed analysis of the observed alloy structures for samples covered with 0.75 ML, 1.5 ML, and 2 ML of Gd, with the substrate temperature in the range from 865 K to 926 K, is presented in Fig. 4. Sub-monolayer Gd

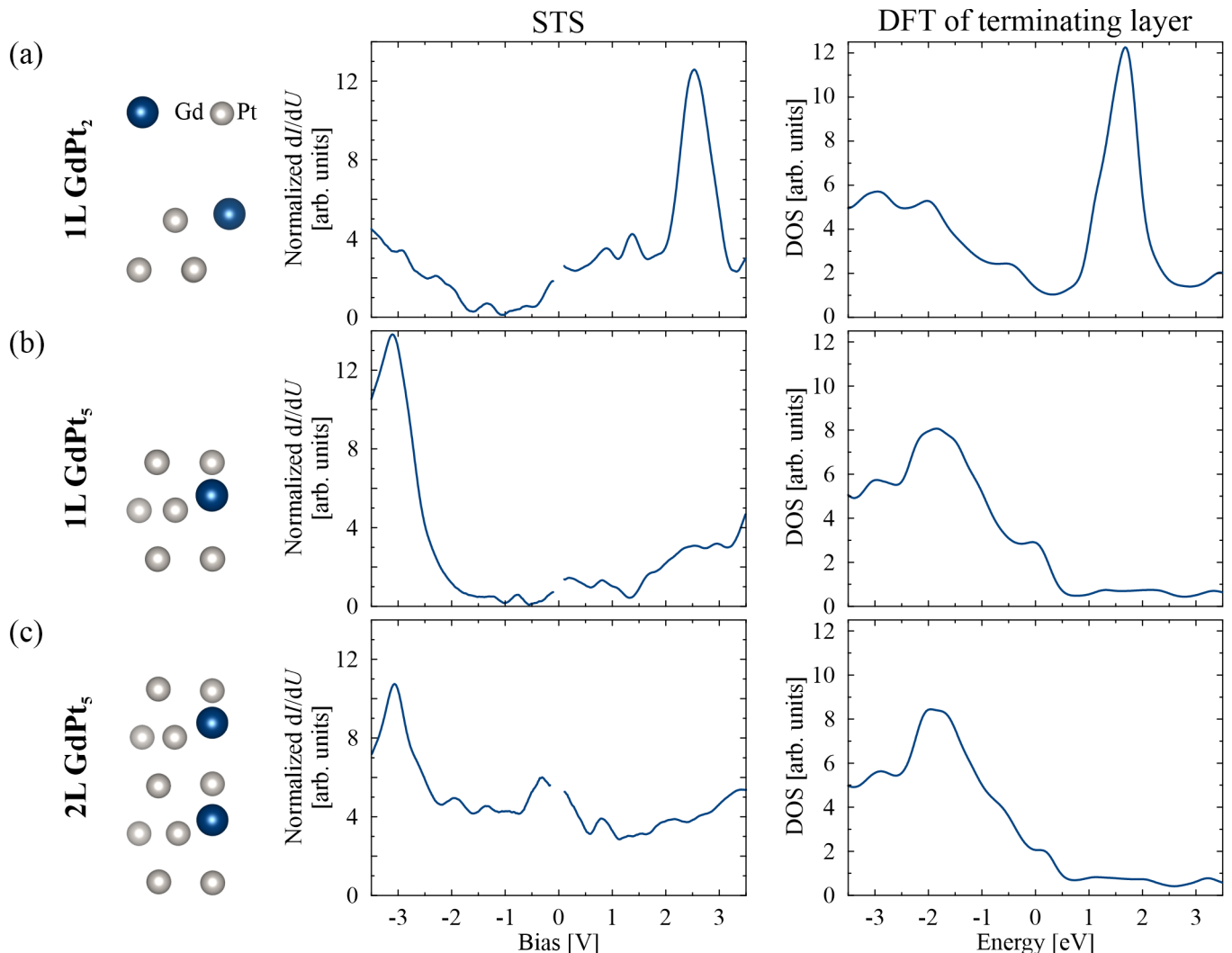


FIG. 2. Rows show top-most layers of the DFT-optimized models, experimental STS data and total DOS of the terminating layer of all three studied alloys: (a) 1L GdPt<sub>2</sub>, (b) 1L GdPt<sub>5</sub>, (c) 2L GdPt<sub>5</sub>.

coverage leads to the most diversified surface in terms of the number of observed structures, thus we could distinguish Gd-Pt clusters as well as all three different surface alloys. We find areas occupied by Gd-Pt clusters and islands only at temperatures up to 880 K. When the substrate temperature increases, the areas occupied by 1L GdPt<sub>2</sub> and Gd-Pt clusters decrease, while simultaneously the 1L GdPt<sub>5</sub> contribution increases. The most obvious explanation for this observation is the increase of atom mobility due to the additional thermal energy. As it was observed before, Pt tends to create overlayers on top of Gd-Pt surface alloys [43, 56]. More specifically, Pt atoms form a kagomé overlayer on top of the GdPt<sub>2</sub> transforming it into 1L GdPt<sub>5</sub>. Interestingly, we observe that the 1L GdPt<sub>5</sub> area increases with increasing temperature at the expense of 2L GdPt<sub>5</sub>.

The sample surface is purely covered with ordered structures when the Gd coverage is greater than 1 ML. 2L GdPt<sub>5</sub> occupies almost 0.67 of the surface when the

amount of deposited Gd corresponds to 1.5 ML coverage (Fig. 4 (b)), while 1L GdPt<sub>2</sub> and 1L GdPt<sub>5</sub> occupy the remaining part of the surface. There is no well-defined trend in area share between these two latter surface alloys. Altogether their share fluctuates around 36% with a prevalence of 1L GdPt<sub>2</sub>. Coverages above 1.5 ML lead to a 2L GdPt<sub>5</sub> dominance on the surface. Regardless of the substrate temperature, it covers almost the whole sample surface when 2 ML of Gd are deposited (Fig. 4 (c)).

#### IV. SUMMARY

In conclusion, we performed a combined STM, STS and DFT investigation of the Gd-Pt intermetallic alloy structures grown on Pt(111). Among the observed structures, we identified three distinct surface alloys, which are single-layer GdPt<sub>2</sub>, single-layer GdPt<sub>5</sub>, and double-layer

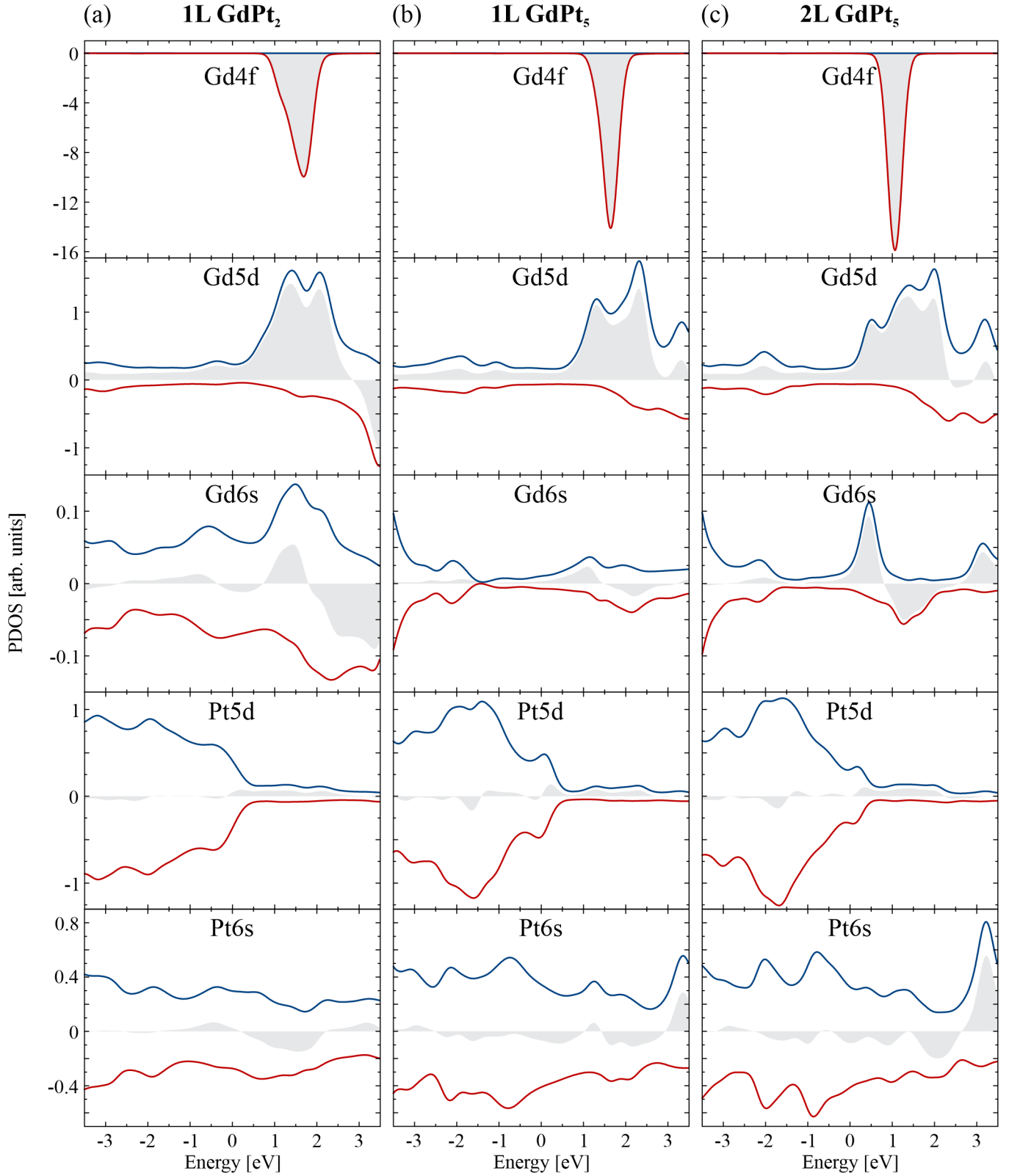


FIG. 3. Electronic structure of Gd-Pt surface alloys. (a), (b), and (c) columns show PDOS plots. The PDOS were calculated for different Gd and Pt states projected onto the terminating layer and in case of GdPt<sub>5</sub> on the Gd closest to the surface for each surface alloy. The red line represents the minority states, the blue line represents the majority states and the gray area in between is the spin asymmetry.

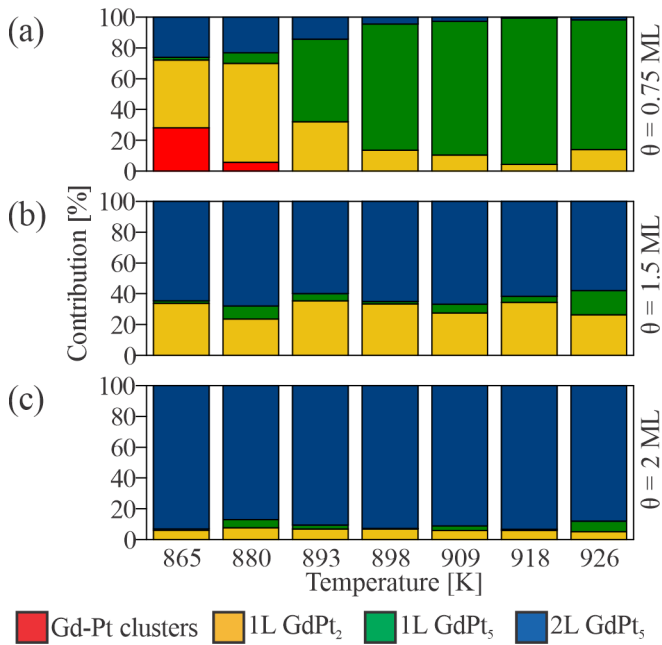


FIG. 4. Temperature-dependent surface area share of different Gd-Pt surface alloys as a function of the substrate temperature in the range from 865 K to 926 K for samples with initial Gd coverage of (a) 0.75 ML, (b) 1.5 ML, (c) 2 ML.

GdPt<sub>5</sub>. The proposed structure of all above-mentioned alloys consists of alternating GdPt<sub>2</sub> and Pt kagomé layers on top of Pt(111). Based on the temperature and coverage dependence of the observed surface structures, we conclude that it is possible to obtain samples almost fully covered with 1L GdPt<sub>5</sub> or 2L GdPt<sub>5</sub>, depending on the growth conditions. The largest area of 1L GdPt<sub>2</sub> is obtained when the initial Gd coverage is 0.75 ML and it requires a temperature ranging from 865 K to 893 K.

1L GdPt<sub>5</sub> grows when the Gd coverage is the same as in the case of 1L GdPt<sub>2</sub>, but it requires a higher temperature (from 898 K to 926 K) to form a kagomé overlayer. 2L GdPt<sub>5</sub> occurs almost exclusively when the initial Gd coverage is 2 ML, independent of the temperature in the analyzed range. Finally, DFT shows a significant spin polarization on both Gd and Pt atoms, which in combination with the quasi-2D nature, and the displacement of Gd from the Pt plane can lead to interesting modifications of the magnetic properties of the GdPt<sub>5</sub> surface alloy compared to its bulk counterpart.

## ACKNOWLEDGMENTS

For funding of this work, we gratefully acknowledge the Office of Naval Research via grant No. N00014-16-1-2900 and the National Science Center Poland via the Sonata Bis project no. 2017/26/E/ST3/00140 and the Preludium project no. 2019/33/N/ST5/01711. The work has been supported in part by the Interdisciplinary Centre for Mathematical and Computational Modelling, University of Warsaw (ICM UW), and the Poznan Supercomputing and Networking Center (PSNC). T.G. acknowledges the Ministry of Education and Science within project 0512/SBAD/2120 realized at Faculty of Materials Engineering and Technical Physics, Poznan University of Technology.

M.B. conceived the experiment. M.P. performed the measurement and analyzed the data. E.S. and M.E. supported the experiment. E.S. performed preliminary data analysis. T.G. supported data analysis. M.H. performed the DFT calculations. M.B., M.P. and M.H. analyzed and interpreted the DFT calculations. R.W. and M.B. supervised the work. M.P., R.W., and M.B. wrote the manuscript. All authors discussed the results and commented on the manuscript.

- 
- [1] K. H. J. Buschow, Intermetallic compounds of rare-earth and 3d transition metals, Reports on Progress in Physics **40**, 1179 (1977).
  - [2] C. C. Chao, H. L. Luo, and P. Duwez, CsCl-type compounds in binary alloys of rare-earth metals with gold and silver, Journal of Applied Physics **34**, 1971 (1963).
  - [3] M. Ohashi, T. Kaneko, S. Miura, and K. Kamigaki, Electric resistivity and thermal expansion of DyAu<sub>2</sub>, Journal of the Physical Society of Japan **34**, 553 (1973).
  - [4] A. A. Gomes and A. P. Guimaraes, Magnetic properties and electronic structure of rare earth-transition metal intermetallic compounds, Journal of Physics F: Metal Physics **4**, 1454 (1974).
  - [5] A. E. Baranovskiy, G. E. Grechnev, I. V. Svechkarev, and O. Eriksson, Electronic structure and magnetic properties of GdM<sub>2</sub> compounds, Journal of Magnetism and Magnetic Materials **258-259**, 520 (2003).
  - [6] S. Miura, T. Kaneko, M. Ohashi, and K. Kamigaki, Magnetic properties of DyAu<sub>2</sub> and DyAg<sub>2</sub>, Journal de Physique Colloques **32**, 1124 (1971).
  - [7] M. Atoji, Magnetic structures of HoAg<sub>2</sub>, The Journal of Chemical Physics **51**, 3877 (1969).
  - [8] E. Weschke, C. Schüssler-Langeheine, R. Meier, A. V. Fedorov, K. Starke, F. Hübinger, and G. Kaindl, Temperature dependence of the exchange splitting of the surface state on Gd(0001): Evidence against spin-mixing behavior, Physical Review Letters **77**, 3415 (1996).
  - [9] R. Pascal, C. Zarnitz, M. Bode, and R. Wiesendanger, Atomic and local electronic structure of Gd thin films studied by STM and STS, Physical Review B - Condensed Matter and Materials Physics **56**, 3636 (1997).
  - [10] D. Weller, S. F. Alvarado, W. Gudat, K. Schröder, and M. Campagna, Observation of Surface-Enhanced Magnetic Order and Magnetic Surface Reconstruction on Gd(0001), Physical Review Letters **54**, 1555 (1985).
  - [11] M. Farle, W. A. Lewis, and K. Baberschke, Detailed analysis of the in situ magnetooptic Kerr signal of gadolinium films near the Curie temperature, Applied Physics Let-



- ters **62**, 2728 (1993).
- [12] H. Tang, D. Weller, T. G. Walker, J. C. Scott, C. Chappert, H. Hopster, A. W. Pang, D. S. Dessau, and D. P. Pappas, Magnetic reconstruction of the Gd (0001) Surface, *Physical Review Letters* **71**, 444 (1993).
- [13] D. Li, C. W. Hutchings, P. A. Dowben, R. Wu, C. Hwang, M. Onellion, A. B. Andrews, and J. L. Erskine, Development of the Gd(0001) band structure with film thickness, *Journal of Applied Physics* **70**, 6565 (1991).
- [14] R. Pascal, C. Zarnitz, H. Tödter, M. Bode, M. Getzlaff, and R. Wiesendanger, Electronic structure of Gd and Tb on W(110) in the submonolayer coverage regime studied by STM and STS, *Applied Physics A: Materials Science and Processing* **66**, 1121 (1998).
- [15] R. Pascal, C. Zarnitz, M. Bode, and R. Wiesendanger, STM-study of Gd/W(110) at submonolayer coverages, *Surface Science* **385**, 990 (1997).
- [16] W. Schneider, S. Molodtsov, M. Richter, T. Gantz, P. Engelmann, and C. Laubschat, Structure and electronic properties of ordered rare-earth (Ce, Dy)-transition-metal (Pd, Rh) surface compounds, *Physical Review B* **57**, 14930 (1998).
- [17] S. Krause, L. Berbil-Bautista, T. Hänke, F. Vonau, M. Bode, and R. Wiesendanger, Consequences of line defects on the magnetic structure of high anisotropy films: Pinning centers on Dy/W(110), *Europhysics Letters* **76**, 637 (2006).
- [18] L. Berbil-Bautista, S. Krause, M. Bode, and R. Wiesendanger, Spin-polarized scanning tunneling microscopy and spectroscopy of ferromagnetic Dy(0001)/W(110) films, *Physical Review B - Condensed Matter and Materials Physics* **76**, 064411(10) (2007).
- [19] M. Bode, R. Pascal, M. Getzlaff, and R. Wiesendanger, Surface state of Gd(0001) films on W(110): Scanning tunneling spectroscopy study, *Acta Physica Polonica A* **93**, 273 (1997).
- [20] R. Pascal, C. Zarnitz, M. Bode, M. Getzlaff, and R. Wiesendanger, Surface electronic structure of Gd (0001) films on W (110), *Applied Physics A: Materials Science and Processing* **65**, 603 (1997).
- [21] M. Getzlaff, M. Bode, S. Heinze, and R. Wiesendanger, New insight into the surface magnetic properties of Gd(0001), *Applied Surface Science* **142**, 558 (1999).
- [22] M. Bode, M. Getzlaff, and R. Wiesendanger, Quantitative aspects of spin-polarized scanning tunneling spectroscopy of Gd(0001), *Journal of Vacuum Science and Technology A: Vacuum, Surfaces, and Films* **17**, 2228 (1999).
- [23] S. A. Nepijko, M. Getzlaff, R. Pascal, C. Zarnitz, M. Bode, and R. Wiesendanger, Lattice relaxation of Gd on W(110), *Surface Science* **466**, 89 (2000).
- [24] M. Getzlaff, R. Pascal, and R. Wiesendanger, Controlled preparation of a magnetic thin film alloy: GdFe<sub>2</sub> and GdFe<sub>3</sub>, *Surface Science* **566-568**, 236 (2004).
- [25] P. Malacrida, M. Escudero-Escribano, A. Verdaguer-Casadevall, I. E. L. Stephens, and I. Chorkendorff, Enhanced activity and stability of Pt-La and Pt-Ce alloys for oxygen electroreduction: the elucidation of the active surface phase, *Journal of Materials Chemistry A* **2**, 4234 (2014).
- [26] M. Corso, M. J. Verstraete, F. Schiller, M. Ormaza, L. Fernández, T. Greber, M. Torrent, A. Rubio, and J. E. Ortega, Rare-earth surface alloying: A new phase for GdAu<sub>2</sub>, *Physical Review Letters* **105**, 016101(4) (2010).
- [27] M. Ormaza, L. Fernández, M. Ilyn, A. Magana, B. Xu, M. J. Verstraete, M. Gastaldo, M. A. Valbuena, P. Gargiani, A. Mugarza, A. Ayuela, L. Vitali, M. Blanco-Rey, F. Schiller, and J. E. Ortega, High temperature ferromagnetism in a GdAg<sub>2</sub> monolayer, *Nano Letters* **16**, 4230 (2016).
- [28] U. Berner and K. D. Schierbaum, Cerium oxides and cerium-platinum surface alloys on Pt(111) single-crystal surfaces studied by scanning tunneling microscopy, *Physical Review B - Condensed Matter and Materials Physics* **65**, 235404(10) (2002).
- [29] J. Kemmer, C. Praetorius, A. Krönlein, P. J. Hsu, K. Fauth, and M. Bode, Structural analysis of the intermetallic surface compound CePt<sub>5</sub>/Pt(111), *Physical Review B - Condensed Matter and Materials Physics* **90**, 195401 (10) (2014).
- [30] M. Ormaza, L. Fernández, S. Lafuente, M. Corso, F. Schiller, B. Xu, M. Diakhate, M. J. Verstraete, and J. E. Ortega, LaAu<sub>2</sub> and CeAu<sub>2</sub> surface intermetallic compounds grown by high-temperature deposition on Au(111), *Physical Review B* **88**, 125405(8) (2013).
- [31] Y. Que, Y. Zhuang, Z. Liu, C. Xu, B. Liu, K. Wang, S. Du, and X. Xiao, Two-Dimensional Rare Earth-Gold Intermetallic Compounds on Au(111) by Surface Alloying, *Journal of Physical Chemistry Letters* **11**, 4107 (2020).
- [32] A. Cavallin, L. Fernández, M. Ilyn, A. Magana, M. Ormaza, M. Matena, L. Vitali, J. E. Ortega, C. Grazioli, P. Ohresser, S. Rusponi, H. Brune, and F. Schiller, Magnetism and morphology of Co nanocluster superlattices on GdAu<sub>2</sub>/Au(111)-(13 × 13), *Physical Review B - Condensed Matter and Materials Physics* **90**, 235419(6) (2014).
- [33] L. Fernández, M. Blanco-Rey, R. Castrillo-Bodero, M. Ilyn, K. Ali, E. Turco, M. Corso, M. Ormaza, P. Gargiani, M. A. Valbuena, A. Mugarza, P. Moras, P. M. Sheverdyaeva, A. K. Kundu, M. Jugovac, C. Laubschat, J. E. Ortega, and F. Schiller, Influence of 4f filling on electronic and magnetic properties of rare earth-Au surface compounds, *Nanoscale* **12**, 22258 (2020).
- [34] L. Fernández, M. Corso, F. Schiller, M. Ilyn, M. Holder, and J. E. Ortega, Self-organized growth of high density magnetic Co nanodot arrays on a Moiré template, *Applied Physics Letters* **96**, 013107(3) (2010).
- [35] L. Fernández, M. Ilyn, A. Magaña, L. Vitali, J. E. Ortega, and F. Schiller, Growth of Co Nanomagnet Arrays with Enhanced Magnetic Anisotropy, *Advanced Science* **3**, 1600187(6) (2016).
- [36] M. Abadía, M. Ilyn, I. Piquero-Zulaica, P. Gargiani, C. Rogero, J. E. Ortega, and J. Brede, Polymerization of Well-Aligned Organic Nanowires on a Ferromagnetic Rare-Earth Surface Alloy, *ACS Nano* **11**, 12392 (2017).
- [37] Y. Que, B. Liu, Y. Zhuang, C. Xu, K. Wang, and X. Xiao, On-Surface Synthesis of Graphene Nanoribbons on Two-Dimensional Rare Earth-Gold Intermetallic Compounds, *Journal of Physical Chemistry Letters* **11**, 5044 (2020).
- [38] C. J. Baddeley, A. W. Stephenson, C. Hardacre, M. Tikhov, and R. M. Lambert, Structural and electronic properties of Ce overlayers and low-dimensional Pt-Ce alloys on Pt(111), *Physical Review B - Condensed Matter and Materials Physics* **56**, 12589 (1997).
- [39] J. M. Essen, C. Becker, and K. Wandelt, Pt<sub>x</sub>Ce<sub>1-x</sub> Surface Alloys on Pt(111): Structure and Adsorption, *Journal of Surface Science and Nanotechnology* **7**, 421

- (2009).
- [40] C. Praetorius, M. Zinner, G. Held, and K. Fauth, Surface termination of CePt<sub>5</sub>/Pt(111): The key to chemical inertness, *Physical Review B* **92**, 195427(5) (2015).
- [41] I. E. Stephens, A. S. Bondarenko, U. Grønbjerg, J. Rossmeisl, and I. Chorkendorff, Understanding the electrocatalysis of oxygen reduction on platinum and its alloys, *Energy and Environmental Science* **5**, 6744 (2012).
- [42] M. Escudero-Escribano, P. Malacrida, M. H. Hansen, U. G. Vej-Hansen, A. Velázquez-Palenzuela, V. Tripkovic, J. Schiøtz, J. Rossmeisl, I. E. L. Stephens, and I. Chorkendorff, Tuning the activity of Pt alloy electrocatalysts by means of the lanthanide contraction, *Science* **352**, 73 (2016).
- [43] M. Escudero-Escribano, A. Verdaguer-Casadevall, P. Malacrida, U. Grønbjerg, B. P. Knudsen, A. K. Jepsen, J. Rossmeisl, I. E. Stephens, and I. Chorkendorff, Pt<sub>5</sub>Gd as a highly active and stable catalyst for oxygen electroreduction, *Journal of the American Chemical Society* **134**, 16476 (2012).
- [44] S. Kuck, J. Wienhausen, G. Hoffmann, and R. Wiesendanger, A versatile variable-temperature scanning tunneling microscope for molecular growth, *Review of Scientific Instruments* **79**, 083903(8) (2008).
- [45] D. Nečas and P. Klapetek, Gwyddion: An open-source software for SPM data analysis, *Central European Journal of Physics* **10**, 181 (2012).
- [46] See Supplemental Material at [URL will be inserted by publisher] for details about averaging spectroscopic data and wide energy range DFT calculations.
- [47] J. A. Stroscio, R. M. Feenstra, and A. P. Fein, Electronic structure of the Si(111)2 × 1 surface by scanning-tunneling microscopy, *Physical Review Letters* **57**, 2579 (1986).
- [48] E. Sierda, M. Elsebach, R. Wiesendanger, and M. Bazarnik, Probing Weakly Hybridized Magnetic Molecules by Single-Atom Magnetometry, *Nano Letters* **19**, 9013 (2019).
- [49] J. Wiebe, F. Meier, K. Hashimoto, G. Bihlmayer, S. Blügel, P. Ferriani, S. Heinze, and R. Wiesendanger, Unoccupied surface state on Pt(111) revealed by scanning tunneling spectroscopy, *Physical Review B - Condensed Matter and Materials Physics* **72**, 193406(4) (2005).
- [50] P. Giannozzi, S. Baroni, N. Bonini, M. Calandra, R. Car, C. Cavazzoni, D. Ceresoli, G. L. Chiarotti, M. Cococcioni, I. Dabo, A. Dal Corso, S. De Gironcoli, S. Fabris, G. Fratesi, R. Gebauer, U. Gerstmann, C. Gougoussis, A. Kokalj, M. Lazzeri, L. Martin-Samos, N. Marzari, F. Mauri, R. Mazzarello, S. Paolini, A. Pasquarello, L. Paulatto, C. Sbraccia, S. Scandolo, G. Sclauzero, A. P. Seitsonen, A. Smogunov, P. Umari, and R. M. Wentzcovitch, QUANTUM ESPRESSO: A modular and open-source software project for quantum simulations of materials, *Journal of Physics Condensed Matter* **21**, 10.1088/0953-8984/21/39/395502 (2009), arXiv:0906.2569.
- [51] P. Giannozzi, O. Andreussi, T. Brumme, O. Bunau, M. Buongiorno Nardelli, M. Calandra, R. Car, C. Cavazzoni, D. Ceresoli, M. Cococcioni, N. Colonna, I. Carnimeo, A. Dal Corso, S. De Gironcoli, P. Delugas, R. A. DiStasio Jr, A. Ferretti, A. Floris, G. Fratesi, G. Fugallo, R. Gebauer, U. Gerstmann, F. Giustino, T. Gorni, J. Jia, M. Kawamura, H.-Y. Ko, A. Kokalj, E. Kucukbenil, M. Lazzeri, M. Marsil, N. Marzari, F. Mauri, N. L. Nguyen, H.-V. Nguyen, A. Otero-de-la Roza, L. Paulatto, S. Ponce, D. Rocca, R. Sabatini, B. Santra, M. Schlipf, A. P. Seitsonen, A. Smogunov, I. Timrov, T. Thonhauser, P. Umari, N. Vast, X. Wu, and S. Baroni, Advanced capabilities for materials modelling with Quantum ESPRESSO, *Journal of Physics: Condensed Matter*, 465901 (2017).
- [52] M. J. Soler, E. Artacho, J. D. Gale, A. Garcia, J. Junquera, P. Ordejón, and S.-P. Daniel, The SIESTA method for ab initio order-N materials simulation, *Journal of Physics: Condensed Matter* **14**, 2745 (2002).
- [53] E. Artacho, E. Anglada, O. Diéguez, J. D. Gale, A. García, J. Junquera, R. M. Martin, P. Ordejón, J. M. Pruneda, D. Sánchez-Portal, and J. M. Soler, The SIESTA method; Developments and applicability, *Journal of Physics Condensed Matter* **20**, 10.1088/0953-8984/20/6/064208 (2008).
- [54] A. García, N. Papior, A. Akhtar, E. Artacho, V. Blum, E. Bosoni, P. Brandimarte, M. Brandbyge, J. I. Cerdá, F. Corsetti, R. Cuadrado, V. Dikan, J. Ferrer, J. Gale, P. García-Fernández, V. M. García-Suárez, S. García, G. Huhs, S. Illera, R. Korytár, P. Koval, I. Lebedeva, L. Lin, P. López-Tarifa, S. G. Mayo, S. Mohr, P. Ordejón, A. Postnikov, Y. Pouillon, M. Pruneda, R. Robles, D. Sánchez-Portal, J. M. Soler, R. Ullah, V. W. Z. Yu, and J. Junquera, Siesta: Recent developments and applications, *The Journal of chemical physics* **152**, 204108 (2020), arXiv:2006.01270.
- [55] J. Tang, J. M. Lawrence, and J. C. Hemminger, Structure and valence of the Ce/Pt(111) system, *Physical Review B* **48**, 15342 (1993).
- [56] E. T. Ulrikkeholm, A. F. Pedersen, U. G. Vej-Hansen, M. Escudero-Escribano, I. E. Stephens, D. Friebe, A. Mehta, J. Schiøtz, R. K. Feidenhansl', A. Nilsson, and I. Chorkendorff, PtxGd alloy formation on Pt(111): Preparation and structural characterization, *Surface Science* **652**, 114 (2016).
- [57] J. L. Smith, Z. Fisk, and R. B. Roof, Ferromagnetism in the RhGd and PtGd systems, *Journal of Applied Physics* **52**, 1684 (1981).